Published in final edited form as:
Mol Pharm. 2014 January 6; 11(1): 49–58. doi:10.1021/mp400523h.

Ultrasound-Mediated Destruction of LHRHa Targeted and Paclitaxel Loaded Lipid Microbubbles for the Treatment of Intraperitoneal Ovarian Cancer Xenografts

Caixiu Pu[#†], **Shufang Chang**[†,*], **Jiangchuan Sun**[#†], **Shenyin Zhu**[#ξ], **Hongxia Liu**[†], **Yi Zhu**[†], **Zhigang Wang**[‡], and **Ronald X. Xu**[†,§]

[†]Department of Obstetrics and Gynecology, Second Affiliated Hospital of Chongqing Medical University, Chongqing 400010, China

[‡]Institute of Ultrasound Imaging, Second Affiliated Hospital of Chongqing Medical University, Chongqing 400010, China

[ξ]Department of Pharmacy, First Affiliated Hospital of Chongqing Medical University, Chongqing 400016, China

[§]Department of Biomedical Engineering, The Ohio State University, Columbus, OH 43210, USA

[#] These authors contributed equally to this work.

Abstract

Ultrasound-targeted microbubble destruction (UTMD) is a promising technique to facilitate the delivery of chemotherapy in cancer treatment. However, the process typically uses non-specific microbubbles, leading to low tumor-to-normal tissue uptake ratio and adverse side effects. In this study, we synthesized the LHRH receptor targeted and paclitaxel (PTX) loaded lipid microbubbles (TPLMBs) for tumor-specific binding and enhanced therapeutic effect at the tumor site. An ovarian cancer xenograft model was established by injecting A2780/DDP cells intraperitoneally in BALB/c nude mice. Microscopic imaging of tumor sections after intraperitoneal injection of TPLMBs showed effective binding of the microbubbles with cancer cells. Ultrasound mediated destruction of the intraperitoneally injected TPLMBs yielded a superior therapeutic outcome in comparison with other treatment options. Immunohistochemical analyses of the dissected tumor tissue further confirmed the increased tumor apoptosis and reduced angiogenesis. Our experiment suggests that ultrasound mediated intraperitoneal administration of the targeted drug-loaded microbubbles may be a useful method for the treatment of ovarian cancer.

Keywords

Microbubbles; ovarian cancer; intraperitoneal injection; ultrasound-targeted microbubble destruction; paclitaxel; luteinizing hormone-releasing hormone

Introduction

Ovarian cancer has the highest mortality among all the gynecological malignancies. It is a silent killer with stable incidence and poor prognosis.[1] The early symptoms of ovarian cancer include abdominal bloating, urinary frequency, a sensation of fullness, and pelvic/

[*]Corresponding author. Mailing address: Department of Obstetrics and Gynecology, Second Affiliated Hospital of Chongqing Medical University, No.74 Linjiang Road, Yuzhong district, Chongqing 400010, China. Tel.: +86 23 6369 3279; fax: +86 23 65104238. shfch2005@163.com..

abdominal pain. Since these symptoms are common and non-specific, they are often overlooked by patients and healthcare professionals until at an advanced stage. The treatment of advanced ovarian cancer usually involves debulking surgery and chemotherapies. However, existing platinum and paclitaxel (PTX) chemotherapies are limited by their non-specific biodistribution, low therapeutic index of anticancer agents, and serious side effects such as neutropenia and neurotoxicity. In order to overcome these limitations, new therapeutic strategies and drug formulations have been investigated.[2] Among these new therapeutic strategies, ultrasonic microbubbles (MBs) have been explored as a promising drug carrier and a drug delivery enhancer.[3-5]

The ultrasound-targeted microbubble destruction (UTMD) technique may offer a number of advantages desirable for targeted delivery of chemotherapy.[6-9] In response to ultrasound (US) pulses, the MBs undergo both stable and inertial acoustic cavitations, induce a variety of dynamic processes[10] (e.g., implosion, microstreaming, shock-wave generation, and microjetting), and cause the disruption of the cell membrane (i.e., sonoporation) that facilitates intracellular uptake of drugs at the target site.[11,12] This mechanism has been utilized in combination with MBs for less invasive and tissue-specific delivery of genes and drugs.[13-22] Furthermore, various disease-targeting ligands have also been coated on the surface of the drug-loaded MBs for the enhanced binding efficiency. Yan et al. loaded LyP-1 peptide and paclitaxel in therapeutic ultrasonic MBs and demonstrated their applications in ultrasound-assisted chemotherapy *in vitro*.[23] We further hypothesize that the drug-loaded MBs with the conjugation of tumor-targeting ligands will bind with the tumor-specific receptors, such as the luteinizing hormone-releasing hormone receptor (LHRH-R), for the enhanced drug deposition at the tumor site while maintaining a low systemic exposure.

LHRH-R is over-expressed in approximately 70% of ovarian cancer cell lines[24] and 80% of ovarian cancers.[25] However, its expression in most of the other visceral organs is negligible.[26] Since natural LHRH is unstable *in vivo*, synthetic LHRH analogue (i.e., LHRHa) with improved bioactivity has been synthesized to target LHRH-R. A number of LHRH analogues are currently in therapeutic use.[27] Previous animal studies have shown that a LHRH-R targeted drug delivery system (DDS) exhibits no pituitary toxicity, insignificant influence on the luteinizing hormone concentration, and negligible effect on the reproductive functions.[26] More recently, Chang et al. coated LHRHa on lipid MBs for ultrasound mediated p53 gene transfection and apoptosis induction in ovarian cancer cells.[28]

In this study, the LHRH-R targeted and PTX-loaded lipid microbubbles (TPLMBs) were synthesized for targeted treatment of ovarian cancer. The TPLMBs exhibit all the important UTMD characteristics comparable to those of the commercially available US contrast agents. Their tumor targeting characteristics and anticancer effects were tested *in vivo* in an intraperitoneal ovarian cancer xenograft model and evaluated by survival analysis as well as immunohistochemical assays. To the best of the authors' knowledge, intraperitoneal administration of tumor-targeted and drug-loaded microbubbles for ultrasound mediated delivery of paclitaxel to intraperitoneally grown ovarian tumor xenografts has not been reported elsewhere.

Materials and Methods

Cell lines and culture

Human ovarian cancer A2780/DDP cells, known to over-express LHRH specific receptors,[29] were a generous gift from Professor Zehua Wang at Wuhan Union Hospital (Wuhan, China). The cells were maintained in a HyClone RPMI 1640 medium (Fisher Scientific, Shanghai, China) supplemented with 10% fetal bovine serum and 0.1%

gentamicin sulfate at 37°C in a humidified incubator containing 5% CO_2. For *in vivo* injection, cells were trypsinized and centrifuged at 800 g for 5 minutes, washed twice, reconstituted in PBS at a concentration of 4×10^7 cells/ml for 200 μL intraperitoneal injections.

Animal model preparation

Four- to five-week-old female BALB/c nude mice were provided by Chinese Academy of Medical Sciences (Beijing, China). The animals were housed in microisolator cages in a pathogen-free animal bio-safety level-2 facility at 22±2°C. Tumors were established by intraperitoneal injection of A2780/DDP cells prepared as above.

All procedures involving the use and care of mice were approved ethically and scientifically by the university in compliance with the Practice Guidelines for Laboratory Animals of China.

Preparation of no-targeted Paclitaxel Loaded MBs(NPLMBs)

5 milligrams of 1,2-dipalmitoyl-sn-glycero-3-phosphatidylcholine (Avanti Polar Lipids Inc., Alabaster, AL, USA), two milligrams of 1,2-distearoyl-sn-glycero-3-phosphatidyl - ethanolamine (Avanti), and two milligrams of PTX (Chengdu Yuancheng Biotechnology Ltd. Co., Chengdu, China) were dissolved in a 1.5 ml vial containing 50 μl of 100 % glycerine and 450 μl of phosphate buffered saline (PBS). The vial was incubated in 40 °C water for 30 minutes, degassed, and reperfused with perfluoropropane gas (C3F8, MW 188 g/mol, Tianjin Institute of Physical and Chemical Engineering, Tianjin, China). The mixture was then mechanically vibrated for 45 seconds in a dental amalgamator (YJT Medical Apparatuses and Instruments, Shanghai, China) at a vibration frequency of 60 Hz. The resultant white mixture was diluted with PBS to obtain the non-targeted and PTX-loaded lipid MBs (NPLMBs).

Preparation of LHRHa-targeted Paclitaxel Loaded MBs (TPLMBs)

LHRHa-targeted and PTX-loaded lipid MBs (TPLMBs) were fabricated by a modified emulsification process consisting of three steps: biotinylating PLMBs (BPLMBs), avidinylating BPLMBs (BSPLMBs), and conjugating BSPLMBs with biotinylated LHRHa peptide. The experimental details for each step are described below. BPLMBs were prepared by replacing 1,2-distearoyl-sn-glycero-3-phosphatidyl-ethanolaminewith 1,2-distearoyl-sn-glycero-3-phosphatidyl-ethanolamine-N-[Biotinyl (Polyethylene Glycol) 2000] (Avanti) in the above recipe. Then those biotinylated NPLMBs (BPLMBs) were washed with PBS solution three times in a bucket rotor centrifuge at 800 g for 3 min to remove excess unincorporated lipids from the MBs. After that, 50 μg of sreptavidin (SA, Beijing Biosynthesis Biotechnology Co., Ltd., China) per 108 MBs was then added to the washed MB dispersion. Following 20 min of incubation at 4°C, the MBs were washed three times under the same centrifugation conditions to remove the unreacted streptavidin and obtain BSPLMBs. After that, the BSPLMBs were incubated at 4° C with 50 μg of biotinylated LHRHa peptides (with amino acid sequence: pGlu-His-Trp-Ser-Tyr-D-leu-leu-Arg-Pro-NH2, synthesized by Beijing SciLight Biotechnology Co. Ltd., Beijing, China) per 10^8 MBs for another 20 mins. Free ligands were removed through washing with PBS. NPLMBs, BNPLMBs and TPLMBs were sterilized by cobalt 60 (60Co) irradiation. Fluorescent microbubbles were prepared according to the same method except that the fluorescent dye DiI 10μl (1 mg/ml, Beyotime Institute of Biotechnology, Jiangsu, China) was added into the lipid mixture during the water bath.

Characterization of TPLMBs

TPLMBs were dispersed in PBS buffer for morphology characterization by a bright field microscope, concentration detection by a blood cell count plate, and size and zeta potential measurement by a Malvern Zetasizer Nano ZS unit (Malvern Instrument, UK). The PTX loading rate was characterized by an Agilent 1100 HPLC system with a Hypersil GOLD C18 column (4.6 mm × 250 mm, 5 μm) and a mobile phase of methanol and PBS mixed at the volume ratio of 70:30. The flow rate was set at 1.0 ml/min and the analysis wavelength was at 228 nm. The standard calibration curve derived from the test showed high linearity, accuracy, and reproducibility, with a correlation coefficient of 0.9991. The drug entrapment efficiency was calculated by the following equation:

$$\text{Drug entrapment efficiency} = (\text{total PTX} - \text{free PTX}) / \text{total PTX} \times 100\%$$

Stability of NPLMBs and TPLMBs

NPLMBs and TPLMBs were storied in 4°C and −20°C, respectively. The MBs were dispersed in PBS for microscopic imaging of morphology at 12 h, 24 h, 48 h, 72 h, 5 d, 7 d, 21 d, and 28d, respectively.

In vivo study of the targeted binding affinity

The binding affinity of the TPLMBs was tested in an intraperitoneally grown ovarian tumor xenograft model and compared with that of the NPLMBs. The xenograft model was established by injecting A2780/DDP cells intraperitoneally in 6 BALB/c nude mice. Three weeks after inoculation, the mice were divided into 2 groups (3 mice per group). Group A was intraperitoneally given 100 μL DiI-labeled NPLMBs diluted in 400 μL PBS, while group B was treated with 100 μL DiI-labeled TPLMBs diluted in 400 μL PBS. 20 minutes after intraperitoneal injection, all the mice were sacrificed. The tumors were excised, frozen in optimum cutting temperature (OCT) compound (Sakura Co., USA), and sectioned serially into slices of 10μm thick. Nuclei were counterstained with DAPI (10μg/ml, Beyotime, Jiangsu, China) for 3 minutes. After washed with PBS, the sections were mounted with anti-fade fluorescent mounting medium (Beyotime, Jiangsu, China) and imaged by a fluorescent microscope (Olympus, Tokyo, Japan).

In vivo study of the anti-tumor effect

UTMD mediated delivery of PTX for ovarian cancer treatment was demonstrated in an intraperitoneally grown ovarian tumor xenograft model. Forty-nine female BALB/c mice were intraperitoneally inoculated with 8×10^6 A2780/DDP cells. Fifteen days after tumor inoculation, the mice were randomly divided into the following seven treatment groups (seven mice per group): (a) control (PBS 500 μL i.p.); (b) applying PTX only (i.e., “PTX only”); (c) applying PTX followed by ultrasound destruction (i.e., “PTX+US”); (d) applying NPLMBs only (i.e., “NPLMBs only”); (e) applying NPLMBs followed by ultrasound destruction (i.e., “NPLMBs+US”); (f) applying TPLMBs only (i.e., “TPLMBs only”); (g) applying TPLMBs followed by ultrasound destruction (i.e., “TPLMBs+US”). PTX was administered every three days at a dose of 20 mg/kg for a total of 15 days (i.e., on days 15, 18, 21, 24, and 27 respectively). For treatment groups (c), (e), and (g), apiezoelectric ceramic unfocused transducer(model CGZZ, Ultrasonographic Image Research Institute, Chongqing Medical University, Chongqing, China) with a diameter of one centimeter and a frequency of 300 KHz was positioned on the abdominal skin of the mice, with the index matched by commercial diagnostic ultrasound gel. Ultrasound pulses were applied to the abdomen for 3 minutes at an average intensity of 1 W/cm^2, duration of 10 seconds, and a duty cycle of 50 %. Two mice in each group were sacrificed 24 hours after the last day of

treatment and the tumors were harvested. Tissue specimens were dissected, placed in 4% paraformaldehyde for preparation of paraffin clines, and snaps frozen for lysate preparation. The rest of the mice were monitored daily for the signs of the reduced physical activity and the progression of the disease. The body weight of the mice was monitored at least three times per week. The survive time of each mouse was recorded.

Tumor apoptosis analysis after *in vivo* treatment

For quantitative assessment of apoptosis, terminal deoxynucleotidyltransferase-mediated dUTP nick end labeling (TUNEL) was carried out with an *in situ* Cell Death Detection Kit (Roche) following the manufacturer's protocol. The cells with brown-stained nuclei were apoptotic. An apoptosis index (AI) was calculated as the percentage of TUNEL-positive cells with respect to the total number of cells evaluated, using five random fields for each of tissue sections at 400 × magnification per group. Slides were quantified in a blind manner by two independent reviewers at two different times.

Apoptosis related protein- caspase-3 expression of the tumor tissue in each group was characterized by western blot analysis. Briefly, samples in each group were homogenized and centrifuged at 12000 g for 30 minutes. The supernatant was separated, and the protein concentration of the lysate was determined with the Bradford protein assay (Bio-Rad, Hercules, CA, USA). For western blot analysis, equal amounts of protein were loaded for sodium dodecylsulfate-poly-acrylamide gel electrophoresis (SDS-PAGE). The protein was then transferred to a nitrocellulose membrane, blocked with PBST (PBS with 0.1% Tween-20) solution containing 5% nonfat milk, and incubated overnight at 4°C with primary antibody against caspase-3 (polyclonal, 1:200, Zhongshan Goldenbridge Biotechnology, Beijing, China). Antibody was detected with horseradish peroxidase-conjugated secondary antibody (1:5000) for one-hour incubation and developed with an enhanced chemiluminescence detection kit. Equal loading was confirmed by glyceraldehyde 3-phosphate dehydrogenase (GAPDH) detection. The Labworks 4.6 software package was used for densitometric analysis.

Detection of VEGF expression and MVD after *in vivo* treatment

Immunohistochemical staining of vascular endothelial growth factor (VEGF) (Biosynthesis Biotechnology Co., Ltd., Beijing, China) and CD34(Kangweishiji Biotechnology, Beijing, China) was performed by an avidin-biotin method 24 hours after the last day of treatment. Briefly, tumor masses were fixed in 4% paraformaldehyde, paraffin embedded, and serially sectioned to the slices of 5μm thick. After the sections were dewaxed and rehydrated using alcohol, the endogenous peroxidase activity was blocked with 3% hydrogen peroxide. The sections were then incubated overnight with the primary antibody in a 4°C humid chamber. For the negative control in each run, PBS was used to replace the primary antibody. After the sections were washed for 3 times with PBS, the specimens were incubated with biotinylated secondary antibody, followed by avidin-biotin peroxidase complex treatment. Microscopic images of the sections were acquired and the VEGF expressions were analyzed by BeiHang Pathological Image Analytical System (Motic China, Xiamen, China)in a blind manner without the operator's interference. Endothelial cells were marked by CD34 and the number of microvessels was counted in five optical fields by microscopy (magnification: 400). The mean value of microvessel density (MVD) was determined by counting the number of microvessels per field.

Statistical analysis

The experimental results were analyzed using a SPSS software package (version 17.0). The *in vitro* measurements were expressed as mean ± standard deviation (SD). The *in vivo* data were analyzed using one-way analysis of variance (ANOVA) method, with the differences

among the means evaluated by the Tukey–Kramer multiple comparison test. Survival rates of different treatment groups were illustrated by the Kaplan-Meier curves and compared by the Log-rank Test. A *P* value of less than 0.05 was considered statistically significant.

Results

Characterization of the synthesized MBs

The size distribution, surface charge, drug loading efficiency, and concentration of the MBs were characterized by the methods as described in reference[30]. The synthesized TPLMBs have a concentration of $(1.1\pm0.1)\times10^9$/ml, a size distribution of (1.8 ± 0.2) μm, a mean zeta potential of −(9.6 ± 3.2) mV, and a drug entrapment efficiency of (73.1 ± 1.6)%. In comparison, the NPLMBs have a concentration of $(1.8\pm0.2)\times10^9$/ml, a size distribution of (1.4 ± 0.3) μm, a mean zeta potential of −(8.5 ± 2.0)mV, and a drug entrapment efficiency of (96.5 ± 1.4)%. No significant morphological difference is observed between the TPLMBs and the NPLMBs. NPLMBs and TPLMBs were less stable when stored in 4°C than −20°C. NPLMBs can be stable when storied in −20°C for 21 days, while TPLMBs were less sable than NPLMB which can only be stored for 72 hours at −20°C.

In vivo characterization of TPLMB's binding affinity

An ovarian cancer xenograft model was established by intraperitoneal injection of A2780/DDP cells in BALB/c nude mice, as shown in Figure 1. Fourteen days after inoculation, the tumor nodules were palpable. Twenty-one days after inoculation, tumors of different sizes were visible throughout the peritoneal cavity. Figure 2 shows the fluorescence microscopic images of the tumor tissue dissected 20 minutes after intraperitoneal injection of DiI-labled NPLMBs and DiI-labeled TPLMBs respectively. According to the figure, TPLMBs target the surface of the LHRH-R positive intraperitoneal tumor with high bind affinity. Incomparison, NPLMBs do not bind with the tumor. This result implies that the LHRH-R targeted and drug-loaded MBs can be intraperitoneally injected and selectively deposited to the surface of a LHRH-R expressed ovarian tumor.

Survival analysis after *in vivo* treatment

Forty-nine nude mice with human ovarian cancer xenografts were randomly divided into 7 groups for different treatments as described in the previous section. By the end of the experiment, all the animals died of the progressive tumor growth with no obvious evidence of cytotoxicity, as measured by eating habits and mobility. Figure 3 plots the survival curves for these 7 groups. According to the figure, the control group (denoted as "PBS") has a median survival time of 31 days, while the other 6 treatment groups exhibit different levels of the extended survival. In comparison with the control, US mediated delivery of targeted PTX-loaded MBs (i.e., "TPLMBs+US"), US mediated delivery of non-targeted PTX-loaded MBs (i.e.,"NPLMBs+US"), direct injection of PTX (i.e., "PTX"), and US mediated delivery of PTX (i.e., "PTX+US") increase the median survival by 52%, 29%, 19%, and 16%, respectively. The "TPLMBs+US" group shows a superior therapeutic outcome with the median survival time significantly longer than other treatments ($P < 0.05$). This implies that the combination of tumor targeting, drug loading by MBs, and US pulse destruction synergistically improves the therapeutic efficiency. The improved therapeutic outcome may be associated with the enhanced drug concentration into the tumor tissue. Among other treatment groups, "NPLMBs+US", "PTX", and "PTX+US" also yield the increased survival time to some extent ($P< 0.05$). However, "NPLMBs" and "TPLMBs" do not affect the animal survival significantly, implying that direct application of PTX-loaded MBs without US mediation(no matter whether they are target or non-target bubbles)does not affect the therapeutic outcome significantly.

Tumor apoptosis and Caspase-3 protein expression after *in vivo* treatment

After the death of each animal, the tumor was dissected and stained for TUNEL assay analysis of apoptosis. Figures 4a to 4g are representative microscopic images of the stained tumor slides for treatment groups (a) to (g) respectively. Cancer cells stained with brown nuclei are apoptotic cells. According to the figure, treatment groups (a), (d), and (f) exhibit weakly positive staining, corresponding to a poor therapeutic outcome. Treatment groups (b), (c), and (e) exhibit moderately positive staining, indicating a moderate antitumor effect. The positive staining in treatment group (g) is the strongest among all the groups, indicating the most effective treatment. Quantitative analysis of the positively stained cells for these treatment groups also yielded the consistent conclusions. According to Figure 5, the apoptosis index (AI) for treatment groups (a),(d), and (f) are less than 20%, whereas those for treatment groups (b), (c), (e), and (g) are (26.40 ± 6.60)%, (27.55 ± 4.46)%, (40.40 ± 4.93)%, (55.94 ± 8.94)%, respectively. Compared with the other treatment groups, group (g) has the highest apoptosis efficiency and the difference is statistically significant (P<0.01). These experiment results indicate that UTMD mediated delivery of TPLMBs significantly increase the tumor apoptosis efficiency.

Tumor apoptosis was evaluated by Western Blot test and immunohistochemistry assay of an apoptosis related protein caspase-3 after each treatment. Figure 6 shows the bright field microscopic images of the caspase-3 stained tumor sections acquired from 7 groups. The positive cells are stained brown in cytoplasm. According to the figure, groups (a), (d), and (f) exhibit weakly positive apoptosis; groups (b), (c), and (e) exhibit moderately positive apoptosis; group (g) exhibits highly positive apoptosis. Quantitative analysis of the area density for the positive cells also yielded the consistent conclusions. According to Figure 7, the area density for treatment groups (a), (d), and (f) are less than 0.1, whereas those for treatment groups (b), (c), (e), and (g) are (0.15 ± 0.01), (0.16 ± 0.01), (0.20 ± 0.01), (0.25 ± 0.04), respectively. Compared with other treatment groups, groups (g) exhibits the strongest expression of Caspase-3 and the difference is statistically significant (P< 0.05). These results indicate that ultrasound mediated delivery of TPLMBs significantly increase the tumor apoptosis efficiency. Figure 8 shows the caspase-3 expression levels for 7 treatment groups obtained by Western Blot analysis. The indexes of caspase-3/GAPDH ratio for treatment groups (a), (d), and (f) are less than 0.05, whereas those for treatment groups (b), (c), (e), and (g) are (0.12 ± 0.02), (0.14 ± 0.02), (0.25 ± 0.04), and (0.42 ± 0.06), respectively. Compared with other treatment groups, group (g) has the highest level of caspase-3 expression (P <0.05), indicating that ultrasound mediated delivery of TPLMBs induces tumor apoptosis.

VEGF and MVD expression

Figures 9a to 9g are bright field microscopic images of the tumor sections with VEGF immunohistochemical staining. The VEGF positive cells are stained brown in cytoplasm. According to the figure, groups (a), (d), and (f) exhibit strong expression of VEGF; groups (b), (c), and (e) exhibit moderate expression of VEGF; and group (g) exhibits low expression of VEGF. Further quantitative analysis yielded consistent conclusions, as shown in Figure 10. According to the figure, the area density of VEGF expression for treatment groups (a), (d), and (f) are more than 0.29; whereas those for treatment groups (b), (c), (e), and (g) are (0.26 ± 0.01), (0.24 ± 0.01), (0.17 ± 0.02), (0.11 ± 0.02), respectively. Compared with other treatment groups, groups (g) has the lowest expression of VEGF and the difference is statistically significant (P< 0.05). These results indicate that ultrasound mediated delivery of TPLMBs significantly hinders tumor angiogenesis. Tumor angiogenesis was also evaluated by a MVD assay with immunohistochemical staining of CD34, as shown in Figure 11. Based on this assay, the number of microvessels per field was quantitatively analyzed for each treatment group and plotted in Figure 12. According to the

figure, “TPLMBs+US” yields a MVD level of (8.3 ± 2.5) microvessels per field, significantly lower than other treatment groups. These results indicate that tumor angiogenesis is significantly inhibited by ultrasound mediated delivery of the tumor targeted and drug-loaded MBs.

Discussion

Targeted delivery of drug-loaded MBs in combination with ultrasound pulse destruction have become a promising therapeutic strategy for the treatment of malignant tumors, atherosclerotic plaques, and thrombi.[30] We have previously coated MBs with tumor-specific ligands to enhance the binding affinity with tumor cells.[28,31] LHRHa peptide has been used to target the corresponding LHRH receptors over-expressed in the plasma membrane of many types of cancer cells.[26,32] PTX is one of the most effective chemotherapeutic drugs for the treatment of various cancers, including ovarian, breast, non-small cell lung cancer, and head and neck carcinomas.[33] We hypothesize that ultrasound mediated delivery of LHRHa-coated and PXT-loaded MBs will facilitate drug deposition at the tumor site for the enhanced therapeutic outcome. This hypothesis has been tested through our *in vitro* and *in vivo* experiments.

Our *in vitro* measurements show that TPLMBs are able to achieve a drug encapsulation efficiency of 73%, similar to that reported by other researchers.[23] The use of the LHRHa peptide to target the over-expressed LHRH receptors in ovarian cancer presents several imaging and therapeutic advantages. First of all, the tumor targeting ligand acts as an anchor to hold the TPLMBs specifically to the tumor site, enabling quantitative tumor detection and image-guided therapy.[34,35] Second, encapsulating multiple contrast agents in TPLMBs may also facilitate multimodal imaging of tumor structural, functional, and molecular characteristics.[36] Third, targeted accumulation and controlled destruction of the TPLMBs at the tumor site will reduce their non-specific distribution in normal tissue and reduce their adverse side effects on healthy organs. Fourth, the targeting moiety and the ultrasound mediation enhance the cellular uptake of the anticancer therapies. Finally, the lipid fragments and the anticancer drugs encapsulated in the MBs remain adherent to the surface of the targeted cancer cells after ultrasonic destruction for the sustained therapeutic effect.[37,23]

Intraperitoneal administration of drug-loaded MBs may provide an effective treatment strategy for many peritoneal cancers and their metastatic lesions. Ovarian cancer is a typical example known to form metastatic lesions along the peritoneal lining, particularly in the advanced stages of the disease.[38] In this study, the metastatic feature of ovarian cancer was modeled by intraperitoneal ovarian cancer xenograft with LHRH-R over-expression. For this cancer model, the therapeutic strategy of intraperitoneal administration and ultrasound mediated destruction of TPLMBs was defined based on the following considerations: (1) Intraperitoneal delivery of drugs and therapeutic radionuclides has been accepted as an effective method to increase the local drug concentration for the treatment of metastatic cancer;[39,40] (2) Intraperitoneal injection of drug-loaded MBs will enhance drug exposure to cancer cells within the peritoneum without increasing the systemic toxicity; (3) With an averaged diameter of (1.8 ± 0.24) μm, our TPLMBs are suitable for intraperitoneal administration instead of intravenous admisntration since MBs with this size cannot effectively penetrate the endothelial fenestration into tumor vasculature;(4)Unlike drug-loaded nanoparticles, MBs with the size of micrometers may achieve the sustained treatment effect in the peritoneal cavity without rapid clearance into the lymphatic drainage.[37,41]

Our *in vivo* experiment demonstrated that US mediation plays a significantly important role in drug delivery. Survival time comparisons among different treatment groups showed that

mice treated by "TPLMBs+US" survived significantly longer than other groups. Even without the targeting ligand, US mediation of NPLMBs (i.e., "NPLMBs+US") also led to significantly extended survival. In comparison, intraperitoneal injection of either NPLMBs or TPLMBs without US mediation does not show significant therapeutic benefit. In our study, ultrasound pulses of 300 KHz were applied to the mice at an average power intensity of 1 W/cm^2 for the duration of 3 minutes. Applying this energy alone may not be sufficient for a significant anti-cancer effect, as evidenced by the previous study that showed no suppression of tumor growth in a SKOV3 ovarian cancer xenograft model after applying US pulses of 240 kHz at an intensity of 7.84 W/cm^2 for 10 minutes.[42] Nevertheless, the mechanism for US mediated delivery of drug-loaded MBs has not been fully understood yet.[43] We believe that the improved anticancer efficiency after US mediation is caused by the enhanced intracellular drug uptake as a result of MB oscillation, fragmentation, and cell membrane disruption.[44,45] The increased intracellular drug uptake is directly responsible for the increased apoptosis and the reduced angiogenesis, as evidenced by our *in vivo* results. In addition, the vascular endothelial cell damage in response to microbubble fragmentation may also contribute to the reduced angiogenesis after treatment.[46,47] Our experiment also showed that intraperitoneal injection of PTX-loaded microbubbles without ultrasonic destruction yielded negligible therapeutic effect, no matter whether the microbubbles were conjugated with the tumor-targeting ligands or not. This phenomenon is different from what has been observed for a nanomicellar formulation or a hetastarch formulation,[48,49] indicating a different mechanism that governs the absorption, distribution, metabolism, and excretion (ADME) characteristics of drug-loaded microbubbles. We hypothesize that the compromised therapeutic effect of the PTX-loaded microbubbles is associated with macrophage endocytosis of the microbubbles, the hindered release of PTX from non-destructed microbubbles to cancer cells, and the short life time of the drug.[50-52] Further experiment is necessary in order to better understand the pharmacokinetics of the intraperitoneally injected PTX-loaded microbubbles and optimize their therapeutic outcome. In this study, no complete recovery was observed for any treated mice because we chose to initiate the treatment on the 15th day after cancer cell inoculation when the tumors were readily palpable. In order to further improve the outcome, we will consider the optimal therapeutic strategies in the future, such as earlier initiation of the treatment, increase of dose, and prolongation of treatment. In our study, the tumor targeting MBs were synthesized by using the biotin-streptavidin interaction. Although this binding strategy has been demonstrated successfully in animal models, its clinical feasibility is challenged by the unwanted immunogenicity. To overcome this limitation, one possible technical approach is to design avidin in the less immunogenic forms.[53,54] The other approach is to use other covalent and non-covalent binding strategies to synthesize tumor targeting microbubbles.[55] Further research and validation efforts are required before these technical advances can be implemented in a clinical setting.

In summary, LHRH receptor targeted and PTX-loaded lipid MBs were successfully synthesized for US mediated therapy of ovarian cancer. *In vivo* experiments in an intraperitoneal ovarian cancer xenograft model demonstrated a promising tumor targeting capability and therapeutic efficiency. Throughout the course of the treatment, no animal showed adverse side effect, indicating the superior safety profile of this promising therapeutic strategy. Although further studies are necessary to understand the therapeutic mechanism and optimize the treatment strategy, the combination of TPLMBs with ultrasound is expected to become a novel drug delivery strategy for targeted chemotherapy of peritoneal malignancies.

Acknowledgments

The authors are grateful to Dr. Pan Li (Institute of Ultrasound Imaging, Second Hospital of Chongqing Medical University, and Chongqing, China) for the helpful technical discussion, Dr. Zehua Wang (Department of Obstetrics and Gynecology, Tongji Medical College, Wuhan Union hospital Huazhong University of Science and Technology, Wuhan, China) for the kind supply of A2780/DDP cells, Dr. Ting Si (University of Science and Technology of China, Hefei, China) for the helpful illustration editing and Dr. Zhibiao Wang (Director of National Engineering Research Center of Ultrasound Medicine, Chongqing Medical University, Chongqing, China) for the generous support of the experimental facilities. This research was supported by Natural Science Foundation of China (81372799), Bureau of Health Foundation of Chongqing (2010-1-6, 2010-1-39), National High Technology Research and Development Program of China (2006AA02Z4FO), and National Cancer Institute (R21CA15977).

References

(1). Cannistra SA. Cancer of the ovary. N Engl J Med. 2004; 351(24):2519–2529. [PubMed: 15590954]

(2). Du Bois A, Pfisterer J. Future options for first-line therapy of advanced ovarian cancer. International Journal of Gynecological Cancer. 2005; 15(Suppl 1):42–50. [PubMed: 15839958]

(3). Geis NA, Katus HA, Bekeredjian R. Microbubbles as a vehicle for gene and drug delivery: current clinical implications and future perspectives. Curr Pharm Des. 2012; 18(15):2166–2183. [PubMed: 22352771]

(4). Kiessling F, Fokong S, Koczera P, Lederle W, Lammers T. Ultrasound microbubbles for molecular diagnosis, therapy, and theranostics. J Nucl Med. 2012; 53(3):345–348. [PubMed: 22393225]

(5). Lentacker I, De Smedt SC, Sanders NN. Drug loaded microbubble design for ultrasound triggered delivery. Soft Matter. 2009; 5(11):2161–2170.

(6). Escoffre JM, Novell A, Serriere S, Lecomte T, Bouakaz A. Irinotecan Delivery by Microbubble-Assisted Ultrasound: In Vitro Validation and a Pilot Preclinical Study. Mol Pharm. 2013

(7). Escoffre JM, Piron J, Novell A, Bouakaz A. Doxorubicin delivery into tumor cells with ultrasound and microbubbles. Mol Pharm. 2011; 8(3):799–806. [PubMed: 21495672]

(8). Florinas S, Nam HY, Kim SW. Enhanced siRNA delivery using a combination of an arginine-grafted bioreducible polymer, ultrasound, and microbubbles in cancer cells. Mol Pharm. 2013; 10(5):2021–2030. [PubMed: 23527953]

(9). Hamano N, Negishi Y, Omata D, Takahashi Y, Manandhar M, Suzuki R, Maruyama K, Nomizu M, Aramaki Y. Bubble liposomes and ultrasound enhance the antitumor effects of AG73 liposomes encapsulating antitumor agents. Mol Pharm. 2013; 10(2):774–779. [PubMed: 23210449]

(10). Wu J, Nyborg WL. Ultrasound, cavitation bubbles and their interaction with cells. Adv Drug Deliv Rev. 2008; 60(10):1103–1116. [PubMed: 18468716]

(11). Pitt WG, Husseini GA, Staples BJ. Ultrasonic drug delivery--a general review. Expert Opin Drug Deliv. 2004; 1(1):37–56. [PubMed: 16296719]

(12). Tsutsui J, Xie F, Porter R. The use of microbubbles to target drug delivery. Cardiovasc Ultrasound. 2004; 2(1):1–7. [PubMed: 14720302]

(13). Kang J, Wu X, Wang Z, Ran H, Xu C, Wu J, Zhang Y. Antitumor effect of docetaxel-loaded lipid microbubbles combined with ultrasound-targeted microbubble activation on VX2 rabbit liver tumors. J Ultrasound Med. 2010; 29(1):61–70. [PubMed: 20040776]

(14). Kinoshita M, Hynynen K. A novel method for the intracellular delivery of siRNA using microbubble-enhanced focused ultrasound. Biochem Biophys Res Commun. 2005; 335(2):393–399. [PubMed: 16081042]

(15). Li P, Zheng Y, Ran H, Tan J, Lin Y, Zhang Q, Ren J, Wang Z. Ultrasound triggered drug release from 10-hydroxycamptothecin-loaded phospholipid microbubbles for targeted tumor therapy in mice. J Control Release. 2012; 162(2):349–354. [PubMed: 22800580]

(16). Mohan P, Rapoport N. Doxorubicin as a molecular nanotheranostic agent: effect of doxorubicin encapsulation in micelles or nanoemulsions on the ultrasound-mediated intracellular delivery and nuclear trafficking. Mol Pharm. 2010; 7(6):1959–1973. [PubMed: 20957997]

(17). Negishi Y, Endo-Takahashi Y, Matsuki Y, Kato Y, Takagi N, Suzuki R, Maruyama K, Aramaki Y. Systemic delivery systems of angiogenic gene by novel bubble liposomes containing cationic lipid and ultrasound exposure. Mol Pharm. 2012; 9(6):1834–1840. [PubMed: 22571418]

(18). Niu C, Wang Z, Lu G, Krupka TM, Sun Y, You Y, Song W, Ran H, Li P, Zheng Y. Doxorubicin loaded superparamagnetic PLGA-iron oxide multifunctional microbubbles for dual-mode US/MR imaging and therapy of metastasis in lymph nodes. Biomaterials. 2013; 34(9):2307–2317. [PubMed: 23276658]

(19). Otani K, Yamahara K, Ohnishi S, Obata H, Kitamura S, Nagaya N. Nonviral delivery of siRNA into mesenchymal stem cells by a combination of ultrasound and microbubbles. J Control Release. 2009; 133(2):146–153. [PubMed: 18976686]

(20). Song S, Noble M, Sun S, Chen L, Brayman AA, Miao CH. Efficient microbubble- and ultrasound-mediated plasmid DNA delivery into a specific rat liver lobe via a targeted injection and acoustic exposure using a novel ultrasound system. Mol Pharm. 2012

(21). Tinkov S, Coester C, Serba S, Geis NA, Katus HA, Winter G, Bekeredjian R. New doxorubicin-loaded phospholipid microbubbles for targeted tumor therapy: in-vivo characterization. J Control Release. 2010; 148(3):368–372. [PubMed: 20868711]

(22). Yan F, Li L, Deng Z, Jin Q, Chen J, Yang W, Yeh CK, Wu J, Shandas R, Liu X, Zheng H. Paclitaxel-liposome-microbubble complexes as ultrasound-triggered therapeutic drug delivery carriers. J Control Release. 2013; 166(3):246–255. [PubMed: 23306023]

(23). Yan F, Li X, Jin Q, Jiang C, Zhang Z, Ling T, Qiu B, Zheng H. Therapeutic ultrasonic microbubbles carrying paclitaxel and LyP-1 peptide: preparation, characterization and application to ultrasound-assisted chemotherapy in breast cancer cells. Ultrasound Med Biol. 2011; 37(5):768–779. [PubMed: 21458148]

(24). Volker P, Grundker C, Schmidt O, Schulz KD, Emons G. Expression of receptors for luteinizing hormone-releasing hormone in human ovarian and endometrial cancers: frequency, autoregulation, and correlation with direct antiproliferative activity of luteinizing hormone-releasing hormone analogues. Am J Obstet Gynecol. 2002; 186(2):171–179. [PubMed: 11854630]

(25). Emons G, Grundker C, Gunthert AR, Westphalen S, Kavanagh J, Verschraegen C. GnRH antagonists in the treatment of gynecological and breast cancers. Endocr Relat Cancer. 2003; 10(2):291–299. [PubMed: 12790790]

(26). Dharap SS, Wang Y, Chandna P, Khandare JJ, Qiu B, Gunaseelan S, Sinko PJ, Stein S, Farmanfarmaian A, Minko T. Tumor-specific targeting of an anticancer drug delivery system by LHRH peptide. Proc Natl Acad Sci U S A. 2005; 102(36):12962–12967. [PubMed: 16123131]

(27). Chabbert-Buffet N, Olivennes F, Bouchard P. GnRH antagonists. Clin Obstet Gynecol. 2003; 46(2):254–264. [PubMed: 12808379]

(28). Chang S, Guo J, Sun J, Zhu S, Yan Y, Zhu Y, Li M, Wang Z, Xu RX. Targeted microbubbles for ultrasound mediated gene transfection and apoptosis induction in ovarian cancer cells. Ultrason Sonochem. 2013; 20(1):171–179. [PubMed: 22841613]

(29). Taratula O, Garbuzenko OB, Kirkpatrick P, Pandya I, Savla R, Pozharov VP, He H, Minko T. Surface-engineered targeted PPI dendrimer for efficient intracellular and intratumoral siRNA delivery. J Control Release. 2009; 140(3):284–293. [PubMed: 19567257]

(30). Bull JL. The application of microbubbles for targeted drug delivery. Expert Opin Drug Deliv. 2007; 4(5):475–493. [PubMed: 17880272]

(31). Xu JS, Huang J, Qin R, Hinkle GH, Povoski SP, Martin EW, Xu RX. Synthesizing and binding dual-mode poly (lactic-co-glycolic acid) (PLGA) nanobubbles for cancer targeting and imaging. Biomaterials. 2010; 31(7):1716–1722. [PubMed: 20006382]

(32). Saad M, Garbuzenko OB, Ber E, Chandna P, Khandare JJ, Pozharov VP, Minko T. Receptor targeted polymers, dendrimers, liposomes: which nanocarrier is the most efficient for tumor-specific treatment and imaging? J Control Release. 2008; 130(2):107–114. [PubMed: 18582982]

(33). Marupudi NI, Han JE, Li KW, Renard VM, Tyler BM, Brem H. Paclitaxel: a review of adverse toxicities and novel delivery strategies. Expert Opin Drug Saf. 2007; 6(5):609–621. [PubMed: 17877447]

(34). Xu RX, Xu JS, Zuo T, Shen R, Huang TH, Tweedle MF. Drug-loaded biodegradable microspheres for image-guided combinatory epigenetic therapy in cells. J Biomed Opt. 2011; 16(2):020507. [PubMed: 21361663]

(35). Zhang L, Xu JS, Sanders VM, Letson AD, Roberts CJ, Xu RX. Multifunctional microbubbles for image-guided antivascular endothelial growth factor therapy. J Biomed Opt. 2010; 15(3):030515. [PubMed: 20614998]

(36). Xu RX. Multifunctional microbubbles and nanobubbles for photoacoustic imaging. Contrast Media Mol Imaging. 2011; 6(5):401–411. [PubMed: 22025340]

(37). Kohane DS, Tse JY, Yeo Y, Padera R, Shubina M, Langer R. Biodegradable polymeric microspheres and nanospheres for drug delivery in the peritoneum. J Biomed Mater Res A. 2006; 77(2):351–361. [PubMed: 16425240]

(38). Lu Z, Wang J, Wientjes MG, Au JL. Intraperitoneal therapy for peritoneal cancer. Future Oncol. 2010; 6(10):1625–1641. [PubMed: 21062160]

(39). de Bree E, Rosing H, Michalakis J, Romanos J, Relakis K, Theodoropoulos PA, Beijnen JH, Georgoulias V, Tsiftsis DD. Intraperitoneal chemotherapy with taxanes for ovarian cancer with peritoneal dissemination. European Journal of Surgical Oncology. 2006; 32(6):666–670. [PubMed: 16618534]

(40). Elit L, Oliver TK, Covens A, Kwon J, Fung MF-K, Hirte HW, Oza AM. Intraperitoneal chemotherapy in the first-line treatment of women with stage III epithelial ovarian cancer. Cancer. 2007; 109(4):692–702. [PubMed: 17238181]

(41). Tsai M, Lu Z, Wang J, Yeh TK, Wientjes MG, Au JL. Effects of carrier on disposition and antitumor activity of intraperitoneal Paclitaxel. Pharm Res. 2007; 24(9):1691–1701. [PubMed: 17447121]

(42). Yu T, Huang X, Hu K, Bai J, Wang Z. Treatment of transplanted adriamycin-resistant ovarian cancers in mice by combination of adriamycin and ultrasound exposure. Ultrason Sonochem. 2004; 11(5):287–291. [PubMed: 15157857]

(43). Luan Y, Faez T, Gelderblom E, Skachkov I, Geers B, Lentacker I, van der Steen T, Versluis M, de Jong N. Acoustical properties of individual liposome-loaded microbubbles. Ultrasound Med Biol. 2012; 38(12):2174–2185. [PubMed: 23196203]

(44). Escoffre JM, Novell A, Piron J, Zeghimi A, Doinikov A, Bouakaz A. Microbubble attenuation and destruction: are they involved in sonoporation efficiency? IEEE Trans Ultrason Ferroelectr Freq Control. 2013; 60(1):46–52. [PubMed: 23287912]

(45). Geers B, Lentacker I, Alonso A, Sanders NN, Demeester J, Meairs S, De Smedt SC. Elucidating the mechanisms behind sonoporation with adeno-associated virus-loaded microbubbles. Mol Pharm. 2011; 8(6):2244–2251. [PubMed: 22014166]

(46). Geers B, Lentacker I, Sanders NN, Demeester J, Meairs S, De Smedt SC. Self-assembled liposome-loaded microbubbles: The missing link for safe and efficient ultrasound triggered drug-delivery. J Control Release. 2011; 152(2):249–256. [PubMed: 21362448]

(47). Hwang JH, Brayman AA, Reidy MA, Matula TJ, Kimmey MB, Crum LA. Vascular effects induced by combined 1-MHz ultrasound and microbubble contrast agent treatments in vivo. Ultrasound Med Biol. 2005; 31(4):553–564. [PubMed: 15831334]

(48). Emoto S, Yamaguchi H, Kishikawa J, Yamashita H, Ishigami H, Kitayama J. Antitumor effect and pharmacokinetics of intraperitoneal NK105, a nanomicellar paclitaxel formulation for peritoneal dissemination. Cancer Sci. 2012; 103(7):1304–1310. [PubMed: 22429777]

(49). Mohamed F, Marchettini P, Stuart OA, Sugarbaker PH. Pharmacokinetics and tissue distribution of intraperitoneal paclitaxel with different carrier solutions. Cancer Chemother Pharmacol. 2003; 52(5):405–410. [PubMed: 12879282]

(50). Bioley G, Bussat P, Lassus A, Schneider M, Terrettaz J, Corthesy B. The phagocytosis of gas-filled microbubbles by human and murine antigen-presenting cells. Biomaterials. 2012; 33(1): 333–342. [PubMed: 21983137]

(51). Choi J, Kim H-Y, Ju EJ, Jung J, Park J, Chung H-K, Lee JS, Lee JS, Park HJ, Song SY, Jeong S-Y, Choi EK. Use of macrophages to deliver therapeutic and imaging contrast agents to tumors. Biomaterials. 2012; 33(16):4195–4203. [PubMed: 22398206]

(52). Hasovits C, Clarke S. Pharmacokinetics and pharmacodynamics of intraperitoneal cancer chemotherapeutics. Clin Pharmacokinet. 2012; 51(4):203–224. [PubMed: 22420577]

(53). Caliceti P, Chinol M, Roldo M, Veronese FM, Semenzato A, Salmaso S, Paganelli G. Poly(ethylene glycol)-avidin bioconjugates: suitable candidates for tumor pretargeting. J Control Release. 2002; 83(1):97–108. [PubMed: 12220842]

(54). Chinol M, Casalini P, Maggiolo M, Canevari S, Omodeo ES, Caliceti P, Veronese FM, Cremonesi M, Chiolerio F, Nardone E, Siccardi AG, Paganelli G. Biochemical modifications of avidin improve pharmacokinetics and biodistribution, and reduce immunogenicity. Br J Cancer. 1998; 78(2):189–197. [PubMed: 9683292]

(55). Klibanov AL. Preparation of targeted microbubbles: ultrasound contrast agents for molecular imaging. Med Biol Eng Comput. 2009; 47(8):875–882. [PubMed: 19517153]

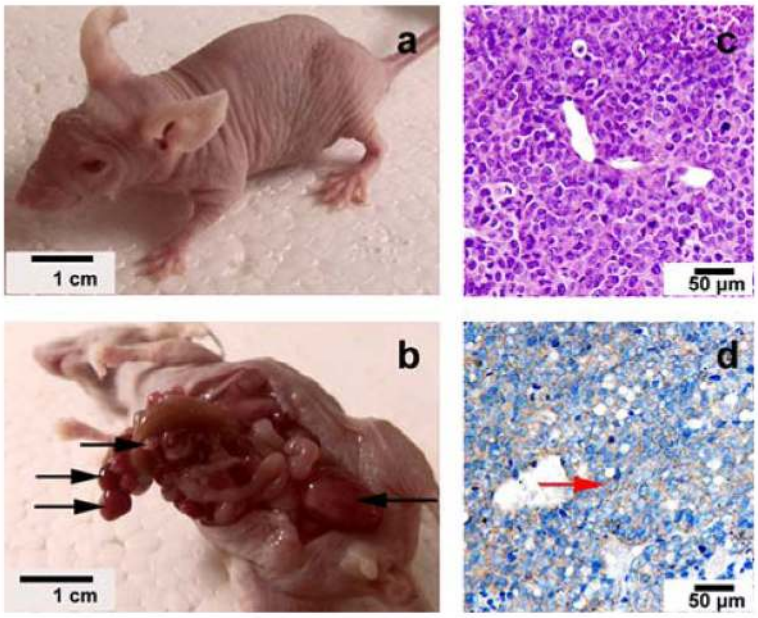

Figure1.

Intraperitonealmode of human ovarian cancer were established in BALB/c nude mice by A2780/DDP cells. Different sizes of tumors (black arrows) throughout peritoneal cavity were observed 21 days after the inoculation (a. before autopsies, b. after autopsies). Tumors were observed by H&E staining (c) and immunohistochemical staining of LHRH-R (d) under microscopy, and the LHRH receptor positive cells were brown in cell membrane(red arrow).

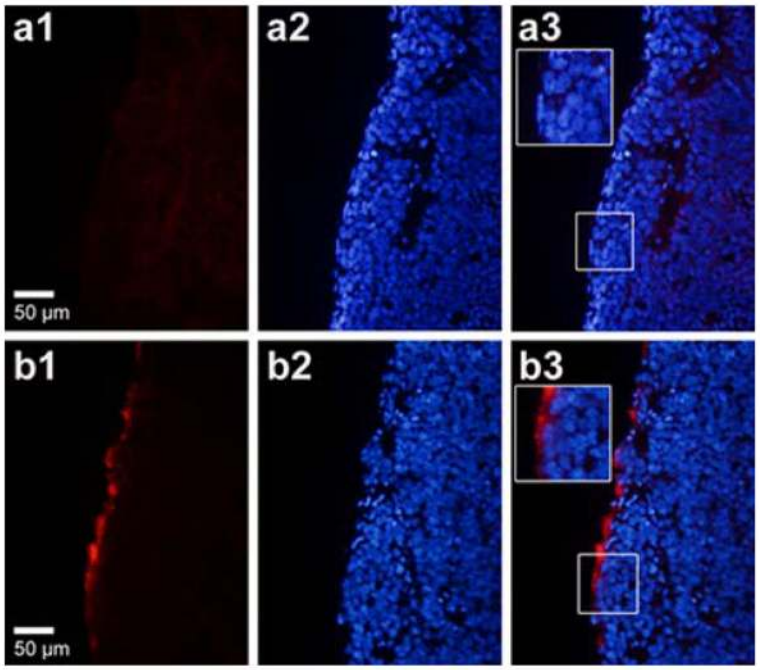

Figure 2.

Intraperitoneal model of human ovarian cancer were established in BALB/c nude mice, 20 min after intraperitoneal injection of DiI-labeled TPLMBs or NPLMBs, tumors were removed to make slide. Red fluorescence was observed under fluorescent microscopy(a1,b1), and red fluorescein was around the edge of slides in TPLMBs group(b1) but we can hardly see red fluorescein around the edge of the slides in NPLMBs group(a1). Nuclei were counterstained with DAPI (a2,b2), and the merge images(a3,b3) shows red fluorescence was still in cytoplasm or plasmalemma (b3).

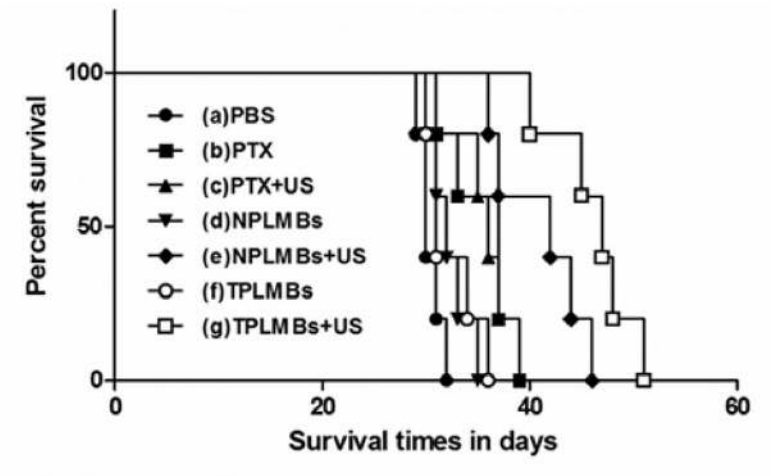

Figure 3.

The survival curves of tumor-bearing mice treated in 7 groups. Mice were implanted with A2780/DDP ovarian tumor cells intraperitoneally. Fifteen days later, mice (5/group) were treated with a single IP injection every 3 days for totally 15 days. The paclitaxel-equivalent dose in drug treated groups was 20 mg/kg. The corresponding median survival times in group (a) to group (g) were 31,37,36,32,42,31 and 47 days. Survival time of mice in group (g) was longer compared with other groups ($P<0.05$).

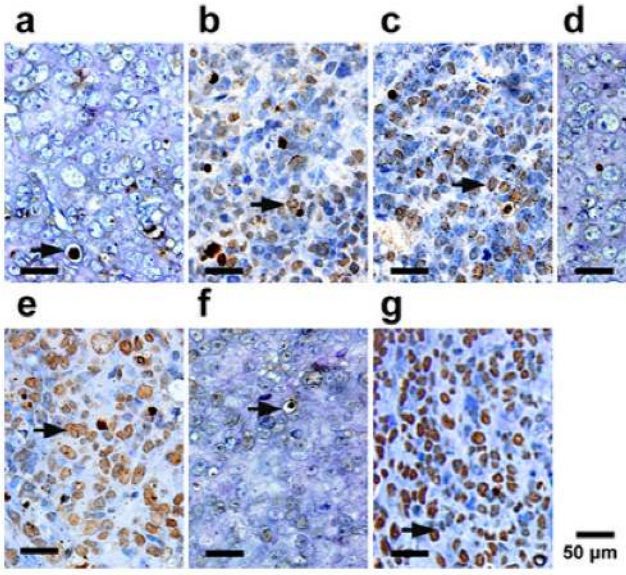

Figure 4.

Sections from each group obtained 24h after treatment from each groups were stained for TUNEL assay. The cancer cells that were brown in nuclei were counted as the apoptotic cells (arrows). Representative slides from each group.

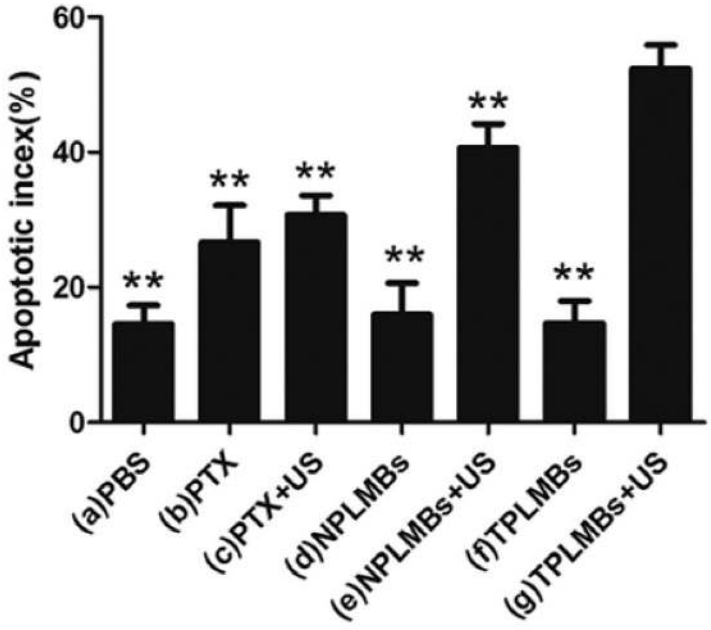

Figure 5.

The apoptotic index in each group. The apoptosis index (AI) for treatment groups (a) to (g) are (14.56 ± 9.35)%, (26.40 ± 6.60)%, (27.55 ± 4.46)%, (15.45 ± 5.95)%, (40.40 ± 4.93)%, (14.75 ± 3.84)%, (55.94 ± 8.94)%, respectively. Compared with group (g), $^{**}P<0.01$.

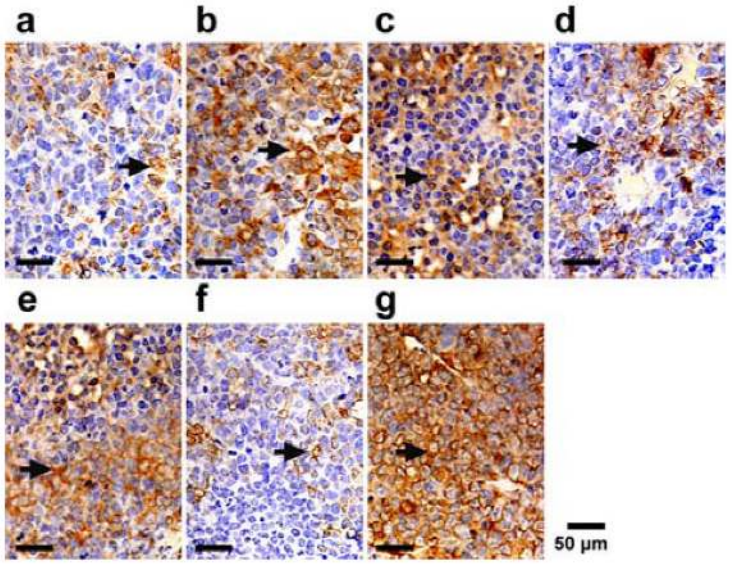

Figure 6.
Caspase-3 immunohistochemical staining was done on tumor sections obtained 24h after treatment from each group. Representative slides from each group. The positive cells were brown in cytoplasm (arrows).

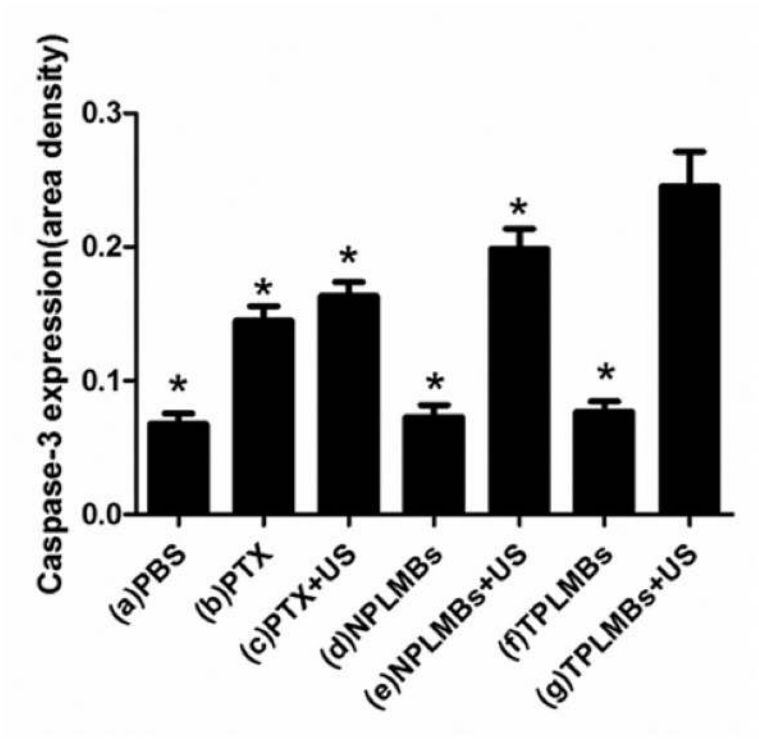

Figure 7.

The slide area density of Caspase-3 protein in each group. The area density of Caspase-3 protein in group (a) to group (g) were (0.07 ± 0.01), (0.15 ± 0.01), (0.16 ± 0.01), (0.07 ± 0.01), (0.20 ± 0.01), (0.08 ± 0.01), (0.25 ± 0.04), respectively. Compared with group (g), **P*<0.05.

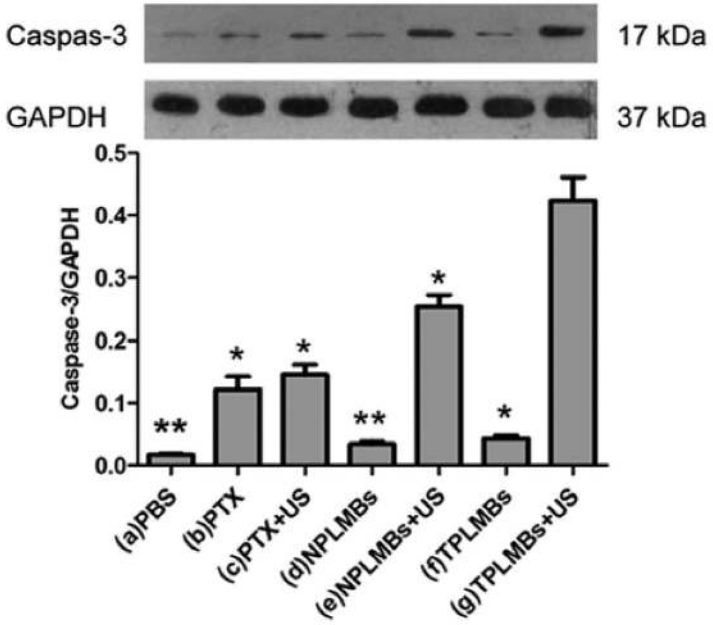

Figure 8.

Caspase-3 expression was detected by western blot analysis. Quantification of band intensity relative to GAPDH was shown in columns. The intensity in group (a) to group (g) were (0.02 ± 0.01), (0.12 ± 0.02), (0.14 ± 0.02), (0.03 ± 0.01), (0.25 ± 0.04), (0.04 ± 0.01) and (0.42 ± 0.06), respectively. Compared with group (g), **P*<0.05, ***P*<0.01.

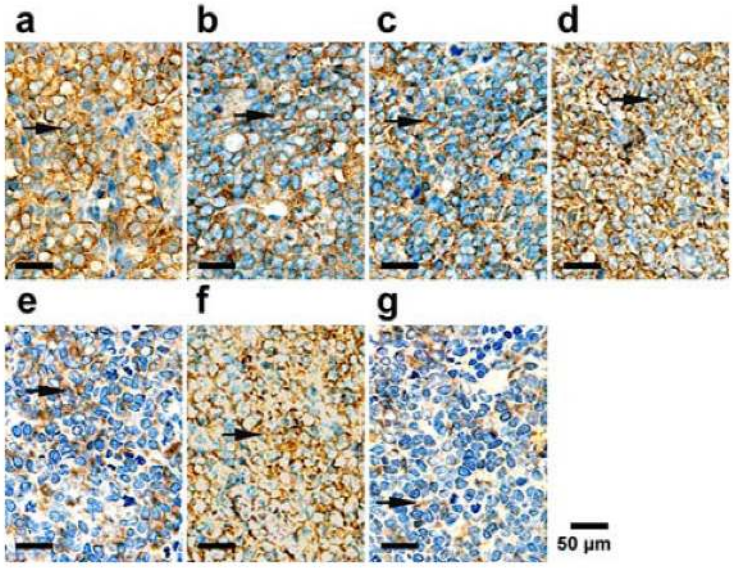

Figure 9.
VEGF immunohistochemical staining was done on tumor sections obtained 24h after treatment from each group. Representative slides from each group. The positive cells were brown in cytoplasm (arrows).

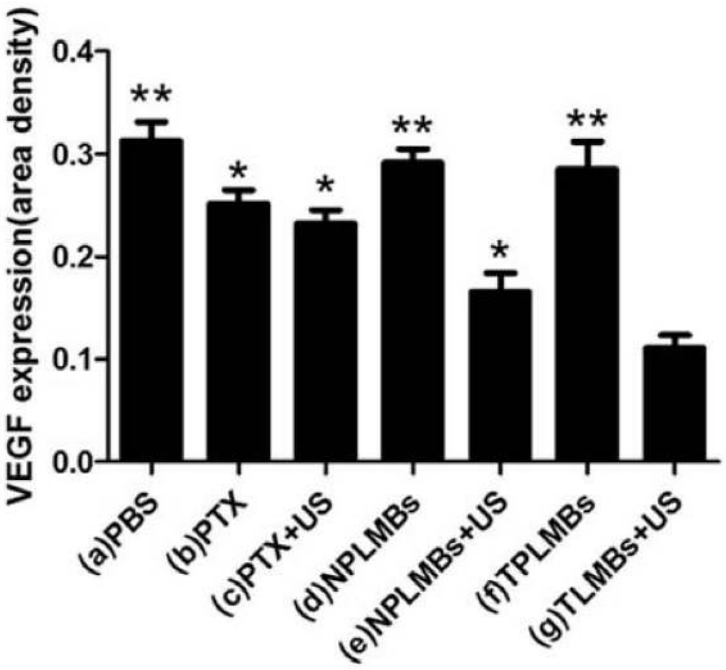

Figure 10.

The slide area density of VEGF protein in each group. The area density of VEGF protein in group (a) to group (g) were (0.31 ± 0.02), (0.26 ± 0.01), (0.24 ± 0.01), (0.29 ± 0.01), (0.17 ± 0.02), (0.29 ± 0.02) and (0.11 ± 0.02), respectively. Compared with group(g), **P*<0.05, ***P*<0.01.

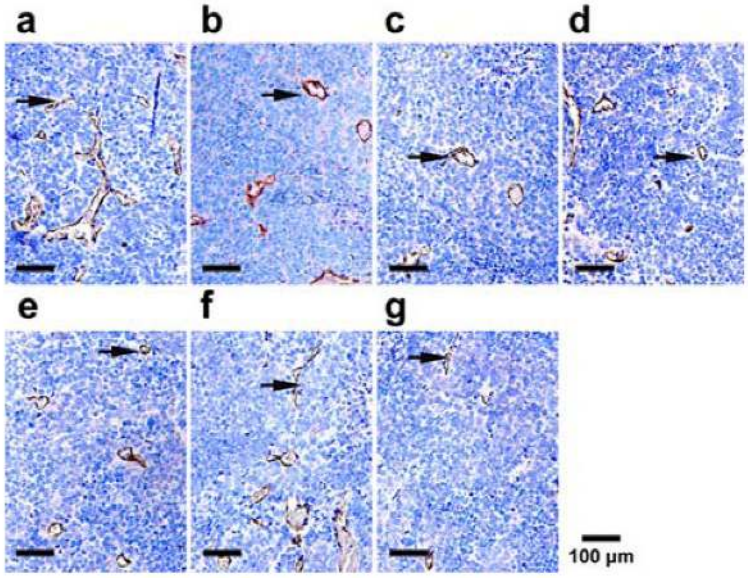

Figure 11.
MVD were determined 24h after treatment by immunohistochemical staining of CD34. The number of vessels per ×200 field were counted. Representative slides from each group. Arrows show the positive microvessels.

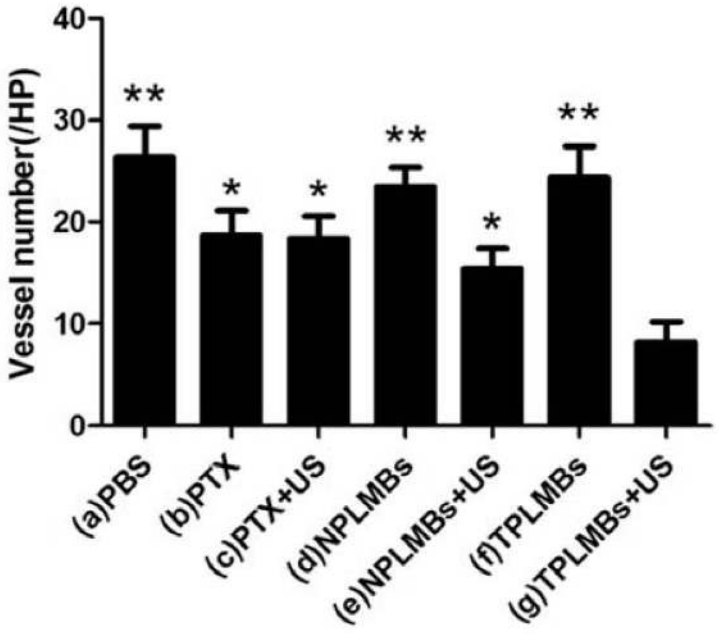

Figure12.

Quantitative analysis of the number of microvessels in each group. The MVD in group (a) to group (g) were (26.4 ± 3.2), (18.5 ± 5.4), (18.3 ± 2.3), (23.5 ± 2.3), (13.5 ± 4.2), (24.4 ± 3.0) and (8.3 ± 2.5), respectively. Compared with group TPLMBs+US, **P*<0.05, ***P*<0.01.